Atmos. Meas. Tech. Discuss., 5, 979–1001, 2012
www.atmos-meas-tech-discuss.net/5/979/2012/
doi:10.5194/amtd-5-979-2012

Atmospheric Measurement Techniques Discussions

Improved retrieval of SO_2 from Ozone Monitoring Instrument: residual analysis and data noise correction

H. Yan[1,2], L. Chen[1], J. Tao[1], L. Su[1], and D. Han[1]

[1]State Key Laboratory of Remote Sensing Science, Jointly Sponsored by the Institute of Remote Sensing Applications of Chinese Academy of Sciences and Beijing Normal University, Beijing, China
[2]Graduate University of the Chinese Academy of Sciences, Beijing, China

Received: 9 January 2012 – Accepted: 11 January 2012 – Published: 27 January 2012

Correspondence to: L. Chen (lfchen@irsa.ac.cn)

Published by Copernicus Publications on behalf of the European Geosciences Union.

Abstract

In this study, based on Ozone Monitoring Instrument (OMI) observation data and considering the shortage of current Band Residual Difference algorithm (BRD) algorithm in data noise correction since late 2008, we make a detailed analysis of OMI SO_2 main noise sources and determine the best residual adjustment area by analyzing the different residual correction effects. After such modification, the OMI SO_2 PBL results noise which use BRD retrieval algorithm is largely reduced, the precision of the SO_2 results is improved, and the optimization of the BRD algorithm for data noise is realized. We select China as our study area and compare the results between the optimized results and the OMI SO_2 PBL products. Results show that they are consistent with each other in January 2008; however, our modified algorithm results have higher precision and more reliable SO_2 spatial distribution in January 2009. Finally, other current retrieval error sources are discussed, and further research is needed on these areas.

1 Introduction

Sulfur dioxide (SO_2) is an important index to urban atmospheric quality evaluation. The spatiotemporal changes of SO_2 have a significant impact on the environment and the climate. The natural sources of SO_2 are sulfur minerals decomposition, oxidation of dimethyl sulfate from marine phytoplankton, and degassing and eruptions of volcanoes. Anthropogenic activities also increase the SO_2 concentration in the atmosphere. These anthropogenic activities include the smelting of sulfur ore, combustion of coal, emission of motor vehicle, and industrial activities (Cullis and Hirschler, 1980).

Since the Nimbus-7 Total Ozone Mapping Spectrometer's (TOMS) first sighting of SO_2 cloud from the El Chichón's eruption in 1982 (Krueger, 1983), satellite remote sensing technology has begun to play an important role in the field of atmospheric monitoring. Later, Global Ozone Monitoring Experiment (GOME), SCanning Imaging

Absorption spectroMeter for Atmospheric CartograpHY (SCIAMACHY), and Ozone Monitoring Instrument (OMI) were developed, and all these instruments have high SO_2 monitoring capability. Particularly, OMI, which was launched on the EOS/Aura platform in July 2004, combines the hyperspectral measurements of GOME and SCIAMACHY with improved nadir spatial resolution ($13 \times 24\,km^2$), and realizes the daily global monitoring of short-lifetime SO_2. It measures solar radiation backscattered by the earth's atmosphere in the sun-synchronous polar orbit with 1:45 p.m. local equator crossing time, and makes simultaneous measurements in a swath of width about 2600 km, divided into 60 pixels (Levelt et al., 2006). OMI has high sensitivity to anthropogenic SO_2, enabling the acquisition of information of near-surface SO_2 emission; it plays an important role in near-surface anthropogenic SO_2 emission monitoring (Krueger et al., 2002; Krotkov et al., 2008; Carn et al., 2007; Li et al., 2010; Yan et al., 2012).

Methods for retrieval of SO_2 from satellite instruments have been developed and applied to detect volcanic SO_2 for aviation (Yang et al., 2007; Krotkov et al., 2006; Rix et al., 2010; Lee et al., 2008; Corradini et al., 2009; Realmuto et al., 1994). Among the ultraviolet inversion algorithms of SO_2, Differential Optical Absorption Spectroscopy (DOAS) (Platt, 1994; Platt and Stutz, 2008) and Linear Fit algorithm (LF) (Yang et al., 2007) are the ones sensitive to large volcanic SO_2 in the upper troposphere or low stratosphere (Yang et al., 2007; Rix et al., 2010; Lee et al., 2008). Band Residual Difference algorithm (BRD) provides unprecedented measurement sensitivity to near-surface small SO_2 emission (Krotkov et al., 2008; Carn et al., 2007; Li et al., 2010; Yan et al., 2012). The BRD algorithm selects four wavelengths between UV 310.8 nm and 314.4 nm (310.8 nm, 311.9 nm, 313.2 nm, and 314.4 nm), which include the wave crests and wave troughs of SO_2 absorption (Fig. 1). It constitutes three wavelength pairs (P1 = 310.8–311.9 nm, P2 = 311.9–313.2 nm, and P3 = 313.2–314.4 nm), and uses OMI O_3 column amount and Lambertian Effective Reflectivity (LER) to estimate the total vertical column amount SO_2 (Krotkov et al., 2006). With high sensitivity to SO_2, BRD can detect the changes of small anthropogenic SO_2 emission in the Planetary Boundary Layer (PBL), which has a significant impact on environment monitoring

Discussion Paper | Discussion Paper | Discussion Paper | Discussion Paper |

AMTD

5, 979–1001, 2012

Improved retrieval of SO_2 from Ozone Monitoring Instrument

H. Yan et al.

Title Page

Abstract Introduction

Conclusions References

Tables Figures

◀◀ ▶▶

◀ ▶

Back Close

Full Screen / Esc

Printer-friendly Version

Interactive Discussion

and climate change. However, the current BRD algorithm does not have sufficient capability to noise correction processing, and the OMI SO_2 PBL product which uses BRD retrieval algorithm shows clear track noise since late 2008, which is unfavorable for OMI SO_2 PBL product application.

Considering the shortage of the current BRD algorithm for data noise correction, we develop a new optimization method. Through the detailed analysis of OMI SO_2 main noise sources, we determine the best residual adjustment area by analyzing the different residual correction effects. After such optimization, the OMI-retrieved SO_2 results noise of the BRD algorithm was largely reduced, the precision of the SO_2 results was improved, and the optimization of the BRD algorithm for data noise was realized. We chose China as our study area and compared the results between the optimized results and the OMI SO_2 PBL products. Results show that former has higher precision and reasonable SO_2 vertical total amount distribution. For the present study, we used data from the National Aeronautics and Space Administration (NASA) Goddard Earth Sciences Data and Information Services Center (GESDISC).

2 Data noise sources and residual analysis

By using the above-mentioned BRD SO_2 retrieval method, OMI level 1 solar irradiance and earth radiance data (Van den Oord et al., 2002), and OMI level 2 O_3 column amount data (Bhartia and Wellemeyer, 2002), we obtain the vertical total column SO_2 in the atmosphere (DU = Dobson Units or milli atm cm, 1 DU = 2.69×10^{16} molecules cm^{-2}). Figure 2 shows the SO_2 column amount results by using the OMI level 1 solar irradiance (orbit 18 570), earth radiance data (orbits 18 565 and 18 566), and OMI level 2 O_3 products (orbits 18 565 and 18 566) on 11 January 2008. Without solar irradiance correction and residual correction, the retrieved SO_2 column amount results show several clear stripes, which are outlier values in the atmosphere SO_2 column data as a function of the viewing angle (Fig. 2a–d). These regularly

AMTD
5, 979–1001, 2012

distributed stripes noises mask the effective signals, including SO_2 absorption information. Therefore, to get the reasonable global distribution of SO_2 and enable OMI SO_2 application, it is necessary to mitigate these stripes noise.

OMI uses the sun-synchronous polar orbit with a daily global coverage and a solar irradiance corresponding to about 14 earth radiances in one day measurement. When the same solar irradiance data (orbit 18 570) are applied to different earth radiance data (orbits 18 565 and 18 566) in one day, the SO_2 column amount distribution shows a clear along-track stripes error because of the invalid value in the solar irradiance data. We used the nearest neighbor interpolation method to remove the invalid value in the solar irradiance data, and the clear stripes error can be removed, as shown in Fig. 2c, d. However, even after such reprocessing, the SO_2 column amount remains to have along-track noise. Different earth measurement orbits in one day show the coincident stripes distribution, similarly performing at some certain observation angles, as shown in Fig. 2c, d. Considering the OMI observation mode, these SO_2 along-track stripes mainly come from solar irradiance noise, which is affected by dark signal, diffuser features, and signal noise, among others (Veihelmann and Kleipool, 2006). These noises in solar irradiance are not constant; rather, they change over time.

Apart from solar irradiance noises, the earth radiance data noises also introduce cross-track noise into the SO_2 column amount results. As OMI sensor ages, the earth radiance data are affected by the row anomaly effect since late 2008. This row anomaly effect causes four distinct errors on earth radiance: a multiplicative error by blockage effect, which causes the radiance value to decrease; a wavelength shift error; a stray earthlight related additive error, which causes the radiance value to increase; and a stray sunlight related additive error, which causes the radiance value to increase (http://www.knmi.nl/omi/research/product/rowanomaly-background.php). The OMI row anomaly is dynamic, which means that it varies with time.

In the process of SO_2 retrieval, the residual, as an intermediate value, is the result of the measured reflection subtracted from the simulated reflection at the top of the atmosphere, and determines the final SO_2 result. It is affected by many factors, including

AMTD
5, 979–1001, 2012

solar irradiance noise, earth radiance noise, O_3 data noise, SO_2 and O_3 absorption spectrum, satellite observation geometry, and other error sources. To mitigate these noise interferences, background correction for residual is needed before calculating the SO_2 vertical column amount.

The DOAS retrieval algorithm uses a reference sector method by subtracting the presumably SO_2 free reference data on the same day at the same latitude (Khokhar et al., 2005; Richter et al., 2006). However, the forward model errors or satellite measurement errors that affect the SO_2 retrieval results are dynamic over the world and correlate with time, observation geometry, O_3 amount, and surface reflectivity, among others. Therefore, using the fixed reference sector for the empirical correction of SO_2 retrieval possibly bring new error sources. Yang K developed a sliding median method for residual correction, which has been applied to OMI SO_2 products (Krotkov et al., 2008; Yang et al., 2007). It calculates the median residual for each cross-track pixel from a sliding group pixels covering about 30° latitude along the orbit track, and then subtract the sliding median value for each spectral band and each cross-track position, to reduce the error interference for the centered pixels. This method can reduce any cross-track and along-track biases. This method enables the relative SO_2 distribution, and not the absolute SO_2 results. As seen in Fig. 2e, f, after residual correction, the along-track stripes were largely reduced. In addition, the quality of the OMI SO_2 PBL data on 11 January 2008, is relatively reliable and has low signal-to-noise ratio; however, since 2009, as the OMI sensor ages, the SO_2 products have been seriously affected by row anomaly. Moreover, data noises emerge largely in China, which cannot be effectively corrected by the current SO_2 BRD retrieval algorithm (Krotkov et al., 2006) (Fig. 3). These high-value noises were clearly erroneous, making the SO_2 results unreliable on that day. We provided a new scheme for the BRD SO_2 retrieval algorithm, which reduced the BRD SO_2 results noise, improved the precision of the BRD SO_2 results, and enabled the reasonable SO_2 vertical column amount distribution.

By selecting an area free of SO_2, over the North Pacific Ocean area (0–30° N, 140–170° E), we took the first wavelength pair as an example and selected pixels with SO_2

AMTD
5, 979–1001, 2012

slant column less than 2 DU; we analyzed the different residual correction area effects. Figure 4 shows that the median value of the residual for residual correction from a sliding group pixels covering 20° or 10° latitude is consistent with the results covering 30° latitude in the cross-track direction on 16 January 2008; meanwhile, the median residual from the 5° latitude sliding group pixels is not sufficient to include the background error. When the selected pixel is near the terminator with high solar zenith angle, the terminator data with high noise for residual correction will result in the worsening of the selected pixel retrieval result. Hence, it is important to determine the residual correction area. As shown in Fig. 3, with 30° latitude residual correction area, the OMI SO_2 PBL product yields clear cross-track noises in January 2009. From the residual analysis on 12 January 2009, as shown in Fig. 5, the median value from 30° latitude residual correction area has an abnormally low value in the 40 pixel position at the cross-track direction, which largely deviates from the uncorrected residual for the centered pixel. With such outlier median value for residual correction, the SO_2 retrieval results will show spike value at the cross-track direction. The median value from 20° latitude residual correction area also has a low value in the 40 pixel position, whereas 10° latitude median value did not record a low value. Therefore, the median value from 10° latitude residual correction area has a relatively better residual correction effect.

In this study, we used the modified residual correction scheme to reduce the SO_2 column amount noise and improve the precision of the BRD SO_2 algorithm retrieval results. In detail, by using the TOMS forward model TOMRAD (Dave, 1964), we calculated the residual at four wavelengths between UV 310.8 nm and 314.4 nm (310.8 nm, 311.9 nm, 313.2 nm, and 314.4 nm) and assumed the air mass factor (AMF) value as a constant 0.36; we used the SO_2 absorption cross-section data at a constant temperature (273 K) (Bogumil et al., 2003) and calculated the median residual value from a sliding group of 10° latitude residual correction area. Comparing with the mean residual value, the median value is less sensitive to the outlier value. When the selected pixels are near the terminator, we decrease the residual correction area. Bad pixels determined by residuals are filtered before median residual value calculation. Finally,

AMTD
5, 979–1001, 2012

by subtracting the corresponding median residual value, we obtained the corrected residual and then used these corrected residual to retrieve the SO_2 column amount.

3 Results and discussion

By selecting OMI level 1 and level 2 products in China on 9, 11, 12 and 16 January 2008, we analyzed the space distribution coherence and correlation of the SO_2 column amount between the modified algorithm results and the OMI released SO_2 PBL products. The period chosen is during the Chinese winter, which has a low near-surface temperature, with the SO_2 average conversion rate in the atmosphere being lower than that in the summer (Eatough et al., 1982; Khoder, 2002); during this period, anthropogenic activities are increasing (like coal heating) – factors that make SO_2 emission higher than in the summer – which is a more effective reflection of regional anthropogenic SO_2 emission and is easily detected by satellite. In this study, we chose China as the research area. Since the last century of the 1980s, after China's reforms and opening up, the Chinese economy has rapidly boomed and changed from an agriculture country to an industrial one. However, industrialization and urbanization caused the large emission of pollution gases, greenhouse gases, and particulate matter; the continuous degradation of air quality; and even caused serious environmental pollution incident such as acid rain, haze, and photochemical smog (Chen et al., 2009).

As shown in Fig. 6, in the cross-track direction, the modified BRD SO_2 algorithm results are consistent with the OMI SO_2 PBL product, having similar crest and trough variation in January 2008. However, at the crest of the SO_2 vertical column amount, the absolute value of the modified BRD SO_2 algorithm results is slightly lower than the OMI SO_2 PBL product. This can be caused by several factors, such as background biases subtracted larger, zenith angle interval difference in the forward model, and SO_2 absorption convolving with instrument response function, among others.

We filled the China SO_2 column amount space distribution based on $0.125^\circ \times 0.125^\circ$ latitude-longitude grid, and analyzed the SO_2 column amount space distribution coherence and correlation between the modified algorithm and the OMI level 2 SO_2 PBL product. As shown in Fig. 7, OMI SO_2 PBL product data have high signal-to-noise ratio in January 2008, and the spatial distribution between the modified algorithm and the OMI level 2 SO_2 PBL product has better coherence in the high-value sector than in the low-value sector. The high-value sector is mostly concentrated in Eastern China (e.g., Shandong, Hebei, Henan, and Tianjin) and in the southwest areas of China (e.g., Chongqing and Chengdu). The low-value areas of the modified algorithm are mainly distributed in China Tibet, while OMI level 2 SO_2 PBL products do not show clear low value in the same area. With mass data correlation analysis, the SO_2 column amount of the modified algorithm and the OMI level 2 SO_2 PBL product has good coherence in January 2008 (correlation coefficient R ranges from 0.6674 to 0.8843).

However, since 2009, with the aging of the OMI, satellite signal has begun to attenuate and data noise largely increased; OMI level 2 SO_2 PBL products were affected by the row anomaly effect (Fig. 3). In Fig. 3, OMI level 2 SO_2 PBL products appear to have abnormally high noise in China, which causes the erroneous SO_2 spatial distribution over Inner Mongolia, Shaanxi, Chongqing, Guiyang, and Guangxi. This is unfavorable for OMI SO_2 PBL product application. By using the modified algorithm proposed above, we improved the result of the SO_2 column amount. The modified algorithm effectively removed the unusually high-value noise and obtained the reasonable SO_2 spatial distribution result (Fig. 8). In areas without abnormally high noise, the modified algorithm results and the OMI SO_2 PBL products are consistent, both reflecting the high SO_2 emission of the Chengdu area. This proves that the modified algorithm not only reflects the relativity distribution of SO_2, but also yields higher precision.

By selecting the North Pacific Ocean area (15–20° N, 135–150° E) where we presumed that there are SO_2-free data, we compared the SO_2 results precision between the modified algorithm and the OMI level 2 SO_2 PBL product (Table 1). Without man-made SO_2 emission, the SO_2 column amount should be near zero in this area (Chin et al., 2000). However, because of the sensor measurement and retrieval algorithm errors, the SO_2 column amount value suffered varying degrees of noise interference

AMTD
5, 979–1001, 2012

over the selected area. As shown in Table 1, the precision (standard deviation, σ) of the OMI level 2 SO_2 PBL product data in the selected area is about 1.3 DU, increasing to about 3.4 DU in January 2009, which made the SO_2 results unreliable. After the modification of the algorithm, the SO_2 column amount precision was improved to about 1 DU over the same area during the same period. Meanwhile, temporal and spatial averaging can reduce noise (Krotkov et al., 2008).

4 Conclusions

In this study, we analyzed the OMI SO_2 main noise sources, solar irradiance, and earth radiance, which are regarded as the main measurement error sources. Since 2009, the increasing row anomaly effect has been unfavorable for OMI SO_2 PBL product application. Based on the current BRD SO_2 algorithm and by analyzing the different residual correction effects and determining the best residual adjustment area, we effectively reduced the data noise and realized the optimization of the BRD algorithm. In the present study, we selected China as our study area and compared the results between the optimized and the OMI SO_2 PBL products. Results show that they are consistent with each other in January 2008; however, in January 2009, the modified algorithm results have shown higher precision and more reliable spatial distribution.

Satellite remote sensing technology has incomparable advantages such as a wider coverage area, shorter revisit period, and spatial continuity. However, satellite observation with instantaneous field of view can only obtain transient overpass information; it cannot reflect the continuous temporal variation of atmospheric conditions. Therefore, even with daily global coverage, transient OMI satellite observation cannot precisely reflect the variation of atmospheric conditions in one day. With a short lifetime in the atmosphere, the trace gas SO_2 can rapidly transform to sulfate in several days or even in a few hours (Eatough et al., 1982; McGonigle et al., 2004; Khoder, 2002), demonstrating its clear regional effect. Additionally, SO_2 concentration in the atmosphere – which is affected by natural and anthropogenic emission – varies largely in one day.

AMTD
5, 979–1001, 2012

Therefore, it is necessary to develop joint retrieval through multi-sensor fusion, or combine with atmospheric transport and chemistry model, to obtain the continuous variation of SO_2 in the atmosphere.

In addition to the measurement error, the retrieval algorithm error, which was not discussed in this study, can also bring about more complex noises to the SO_2 result. In this study, we assumed that surface reflectivity is constant for all the retrieval wavelengths. However, such assumption is only a hypothesis for retrieval simplification since, in reality, surface reflectivity varies with wavelength. The gas absorption cross-section data we used were at a constant temperature (273 K), thus temperature variation effect was not considered. In the forward model, there is an overly simplified treatment of many complex processes occurring in a real atmosphere, including Mie scattering by clouds and aerosols. Moreover, the nonlinear effect of the algorithm itself can result in SO_2 result underestimation. All these errors can altogether produce high noise that masks the real SO_2 distribution.

Therefore, although satellite technology can obtain pollutants spatial distribution, source and sink distribution, and transport route, the complex atmosphere conditions cannot be precisely simulated by a simple mathematics, physics model. The quantitative retrieval of satellite monitoring, especially near-surface SO_2 concentration retrieval, needs further study in the future.

Acknowledgements. For this study, we acknowledge the use of OMI level 1 earth radiance and solar irradiance data, as well as OMI level 2 O_3 and SO_2 products from the National Aeronautics and Space Administration (NASA) Goddard Earth Sciences Data and Information Services Center (GESDISC) (http://disc.gsfc.nasa.gov/).

References

Background information about the Row Anomaly in OMI, available at: http://www.knmi.nl/omi/research/product/rowanomaly-background.php, last access: 21 January 2012, 2012.

Bhartia, P. K. and Wellemeyer, C. W.: TOMS-V8 total ozone algorithm, in: OMI Algorithm Theoretical Basis Document, OMI Ozone Products, edited by: Bhartia, P. K., Greenbelt, MD: NASA/Goddard Space Flight Center, 2002.

Bogumil, K., Orphal, J., Homann, T., Voigt, S., Spietz, P., Fleischmann, O. C., Vogel, A., Hartmann, M., Kromminga, H., Bovensmann, H, Frerick, J., and Burrows, J. P.: Measurements of molecular absorption spectra with the SCIAMACHY pre-flight model: instrument characterization and reference data for atmospheric remote-sensing in the 230–2380 nm region, J. Photoch. Photobio. A, 157, 167–184, doi:10.1016/S1010-6030(03)00062-5, 2003.

Carn, S. A., Krueger, A. J., Krotkov, N. A., Yang, K., and Levelt, P. F.: Sulfur dioxide emissions from Peruvian copper smelters detected by the Ozone Monitoring Instrument, Geophys. Res. Lett., 34, L09801, doi:10.1029/2006GL029020, 2007.

Chen, L. F., Tao, J. H., Wang, Z. F., Li, S. S., Han, D., Yu, C., Zhang, Y., and Su, L.: Monitoring of air quality during haze days in Beijing and its surround area during Olympic games, Journal of Atmoshperic and Environmental Optics, 4, 256–265, 2009.

Chin, M., Savoie, D. L., Huebert, B. J., Bandy, A. R., Thornton, D. C., Bates, T. S., Quinn, P. K., Saltzman, E. S., and De Bruyn, W. J.: Atmospheric sulfur cycle simulated in the global model GOCART: comparison with field observations and regional budgets, J. Geophys. Res., 105, 24689–24712, doi:10.1029/2000JD900385, 2000.

Corradini, S., Merucci, L., and Prata, A. J.: Retrieval of SO_2 from thermal infrared satellite measurements: correction procedures for the effects of volcanic ash, Atmos. Meas. Tech., 2, 177–191, doi:10.5194/amt-2-177-2009, 2009.

Cullis, C. F. and Hirschler, M. M.: Atmospheric sulfur- natural and man-made sources, Atmos. Environ., 14, 1263–1278, 1980.

Dave, J. V.: Meaning of successive iteration of the auxiliary equation of radiative tranfer, Astrophys. J., 140, 1292–1303, 1964.

Eatough, D. J., Christensen, J. J., Eatough, N. I., Hill, M. W., Major, T. D., Mangelson, N. F., Post, M. E., Ryder, J. F., Hansen, L. D., Meisenheimer, R. G., and Fischer, J. W.: Sulfur chemistry in a copper smelter plume, Atmos. Environ., 16, 1001–1015, 1982.

Khoder, M. I.: Atmospheric conversion of sulfur dioxide to particulate sulfate and nitrogen diox-

ide to particulate nitrate and gaseous nitric acid in an urban area, Chemosphere, 49, 675–684, 2002.
Khokhar, M. F., Frankenberg, C., Van Roozendael, M., Beirle, S., Kühl, S., Richter, A., Platt, U., and Wagner, T.: Satellite observations of atmospheric SO_2 from volcanic eruptions during the time-period of 1996–2002, Adv. Space Res., 36, 879–887, doi:10.1016/j.asr.2005.04.114, 2005.
Krotkov, N. A., Carn, S. A., Krueger, A. J., Bhartia, P. K., and Yang, K.: Band residual difference algorithm for retrieval of SO_2 from the aura Ozone Monitoring Instrument (OMI), IEEE T. Geosci. Remote, 44, 1259–1266, 2006.
Krotkov, N. A., McClure, B., Dickerson, R. R., Carn, S. A., Li, C., Bhartia, P. K., Yang, K., Krueger, A. J., Li, Z. Q., Levelt, P. F., Chen, H. B., Wang, P. C., and Lu, D.: Validation of SO_2 retrievals from the Ozone Monitoring Instrument over NE China, J. Geophys. Res., 113, D16S40, doi:10.1029/2007JD008818, 2008.
Krueger, A. J.: Sighting of El Chichón sulfur dioxide clouds with the nimbus 7 total ozone mapping spectrometer, Science, 220, 1377–1379, 1983.
Krueger, A. J., Krotkov, N. A., Datta, S., Flittner, D., and Dubovik, O.: SO_2, in: OMI Algorithm Theoretical Basis Document, OMI Trace Gas Algorithms, 2, edited by: Chance, K., Smithsonian Astrophysical Observatory, Cambridge, MA, 49–59, 2002.
Lee, C., Richter, A., Weber, M., and Burrows, J. P.: SO_2 Retrieval from SCIAMACHY using the Weighting Function DOAS (WFDOAS) technique: comparison with Standard DOAS retrieval, Atmos. Chem. Phys., 8, 6137–6145, doi:10.5194/acp-8-6137-2008, 2008.
Levelt, P. F., Van der Oord, G. H. J., Dobber, M. R., Malkki, A., Visser, H., de Vries, J., Stammes, P., Lundell, J. O. V., and Saari, H.: The Ozone Monitoring Instrument, IEEE T. Geosci. Remote, 44, 1093–1101, 2006.
Li, C., Zhang, Q., Krotkov, N. A., Streets, D. G., He, K. B., Tsay, S. C., and Gleason, J. F.: Recent large reduction in sulfur dioxide emissions from Chinese power plants observed by the Ozone Monitoring Instrument, Geophys. Res. Lett., 37, L08807, doi:10.1029/2010GL042594, 2010.
McGonigle, A. J. S., Delmelle, P., Oppenheimer, C., Tsanev, V. I., Delfosse, T., Williams-Jones, G., Horton, K., and Mather, T. A.: SO_2 depletion in tropospheric volcanic plumes, Geophys. Res. Lett., 31, L13201, doi:10.1029/2004GL019990, 2004.
Platt, U.: Differential optical absorption spectroscopy (DOAS), in: Air Monitoring by Spectroscopic Techniques, Chemical Analysis Series, edited by: Sigrist, M. W., John Wiley and Sons, Inc., 127, 27–84, 1994.

AMTD
5, 979–1001, 2012

Platt, U. and Stutz, J.: Differential Optical Absorption Spectroscopy: Principles and Applications, Physics of Earth and Space Environments, Hardcover, Springer, Verlag Berlin Heidelberg, 593 pp., 2008.

Realmuto, V. J., Abrams, M. J., Buongiorno, M. F., and Pieri, D. C.: The use of multispectral thermal infrared image data to estimate the sulfur dioxide flux from volcanoes: a case study from Mount Etna, Sicily, 29 July 1986, J. Geophys. Res., 99, 481–488, doi:10.1029/93JB02062, 1994.

Richter, A., Wittrock, F., and Burrows, J. P.: SO_2 measurements with SCIAMACHY, Atmospheric Science Conference, Eur. Space Agency Cent. for Earth Obs., Frascati, Italy, 8–12 May, 2006.

Rix, M., Valks, P., Van Gent, J., Van Roozendael, M., Spurr, R., Hao, N., Emmadi, S., and Zimmer, W.: Monitoring of volcanic SO_2 emissions using the GOME-2 satellite instrument, EGU General Assembly, Vienna, Austria, 2–7 May 2010, EGU2010-4754, 2010.

Van den Oord, G. H. J., Voors, R. H. M., and De Vries, J.: The Level 0 to Level 1B processor for OMI radiance, irradiance and calibration data, in: OMI Algorithm Theoretical Basis Document, OMI instrument, Level 0-1b processor, Calibration and Operations, edited by: Levelt, P. F., 2002.

Veihelmann, B. and Kleipool, Q.: Reducing Along-Track Stripes in OMI-Level 2 Products, TN-OMIE-KNMI-785, 24 pp., 2006.

Yan, H. H., Chen, L. F., Tao, J. H., Han, D., Su, L., and Yu, C.: SO_2 long-term monitoring by satellite in the Pearl River Delta, Journal of Remote Sensing, in press, 2012.

Yang, K., Krotkov, N. A., Krueger, A. J., Carn, S. A., Bhartia, P. K., and Levelt, P. F.: Retrieval of large volcanic SO_2 columns from the Aura Ozone Monitoring Instrument: comparison and limitations, J. Geophys. Res., 112, D24S43, doi:10.1029/2007JD008825, 2007.

Table 1. Data precision of OMI level 2 SO_2 PBL column amount and modified algorithm SO_2 results in the North Pacific Ocean area.

Sample area (15–20° N, 135–150° E)	Number of pixel	OMI level 2 SO_2 PBL product: Area-averaged SO_2 column amount (DU)	OMI level 2 SO_2 PBL product: Standard deviation (DU)	Modified algorithm SO_2 result: Area-averaged SO_2 column amount (DU)	Modified algorithm SO_2 result: Standard deviation (DU)
Orbit 18 536 (20 080 109)	1953	−0.4852	1.4454	−0.2213	1.1461
Orbit 18 565 (20 080 111)	1695	0.0300	1.2920	−0.1021	1.2721
Orbit 18 580 (20 080 112)	1503	0.3809	1.0892	0.2251	0.6815
Orbit 18 638 (20 080 116)	1984	−0.0999	1.3149	0.3836	1.2998
Orbit 23 779 (20 090 103)	939	1.1351	3.2137	0.1801	0.6801
Orbit 23 910 (20 090 112)	1212	1.4689	3.4634	0.8631	1.0521

AMTD
5, 979–1001, 2012

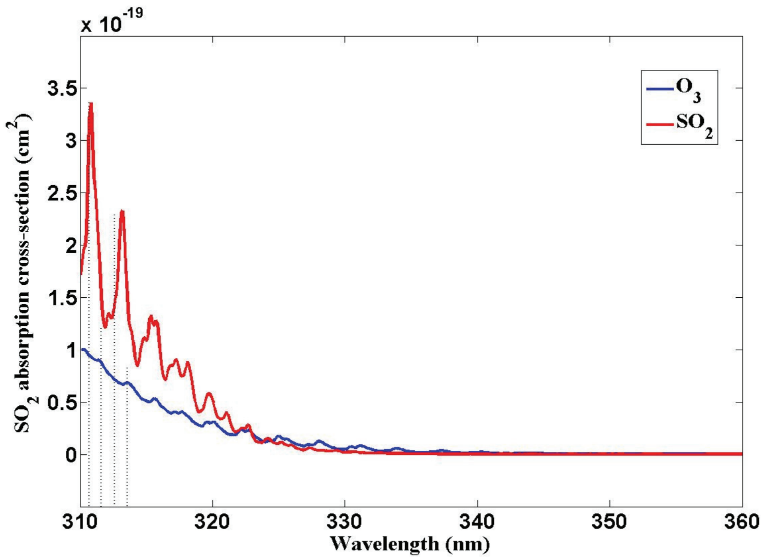

Fig. 1. O_3 and SO_2 absorption spectrum in UV band.

AMTD
5, 979–1001, 2012

Improved retrieval of SO_2 from Ozone Monitoring Instrument

H. Yan et al.

(a) SO_2 stripes caused by invalid solar irradiance value (earth radiance data from orbit 18 565, solar irradiance data from orbit 18 570, and O_3 data from orbit 18 565 on 11 January 2008)

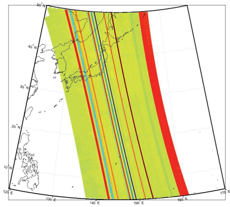

(b) SO_2 stripes caused by invalid solar irradiance value (earth radiance data from orbit 18 566, solar irradiance data from orbit 18 570, and O_3 data from orbit 18 566 on 11 January 2008)

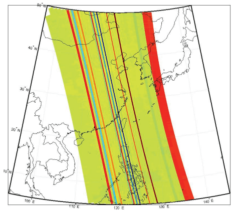

(c) SO_2 stripes caused by solar irradiance noise (earth radiance data from orbit 18 565, solar irradiance data from orbit 18570, and O_3 data from orbit 18 565 on 11 January 2008)

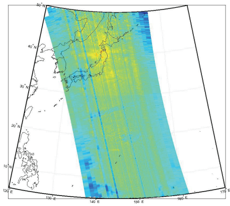

(d) SO_2 stripes caused by solar irradiance noise (earth radiance data from orbit 18 566, solar irradiance data from orbit 18570, and O_3 data from orbit 18 566 on 11 January 2008)

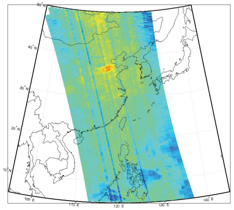

(e) SO_2 results with residual correction (earth radiance data from orbit 18 565, solar irradiance data from orbit 18570, and O_3 data from orbit 18 565 on 11 January 2008)

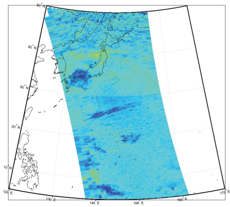

(f) SO_2 results with residual correction (earth radiance data from orbit 18 566, solar irradiance data from orbit 18570, and O_3 data from orbit 18 566 on 11 January 2008)

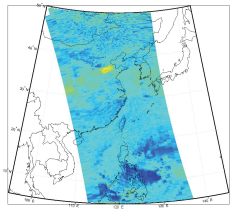

Fig. 2. SO_2 stripes caused by solar irradiance and SO_2 results with residual correction.

AMTD
5, 979–1001, 2012

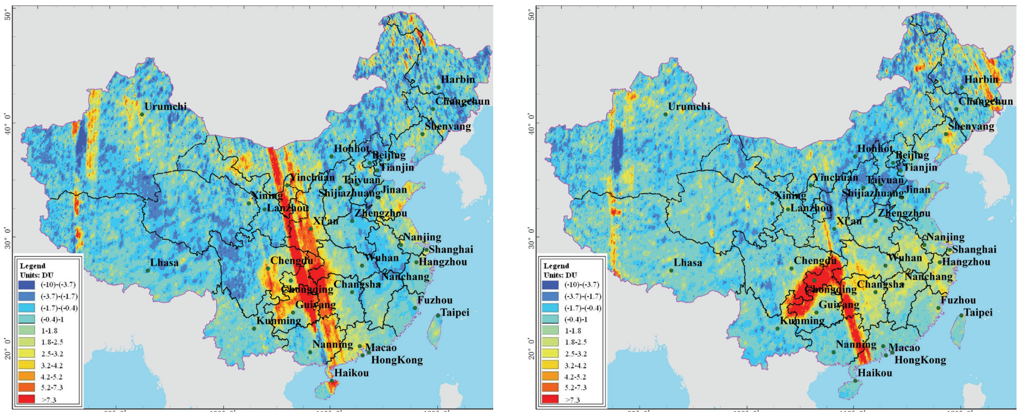

(a) (b)

Fig. 3. OMI level 2 SO_2 PBL high-value noise in China: **(a)** 3 January 2009; **(b)** 12 January 2009.

AMTD
5, 979–1001, 2012

Title Page
Abstract | Introduction
Conclusions | References
Tables | Figures
◀| |▶
◀ ▶
Back | Close
Full Screen / Esc
Printer-friendly Version
Interactive Discussion

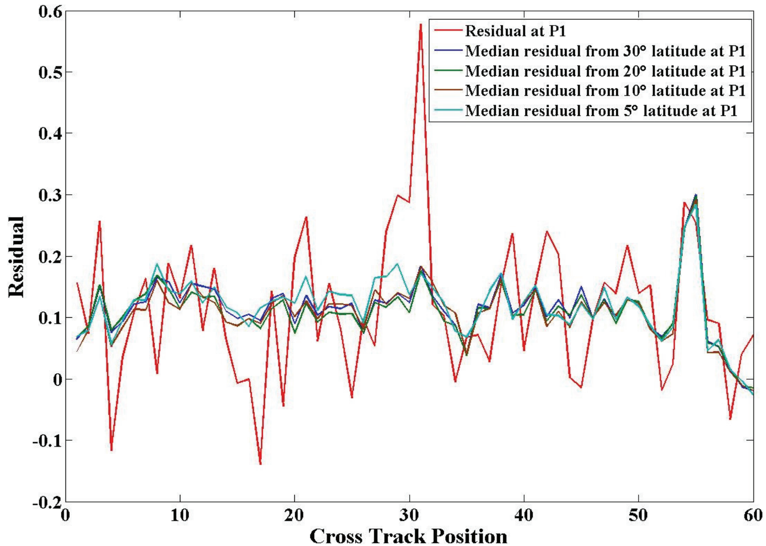

Fig. 4. Residual analysis at the first wavelength pair P1 (orbit 18 637, swath line 1115).

AMTD
5, 979–1001, 2012

Improved retrieval of SO_2 from Ozone Monitoring Instrument

H. Yan et al.

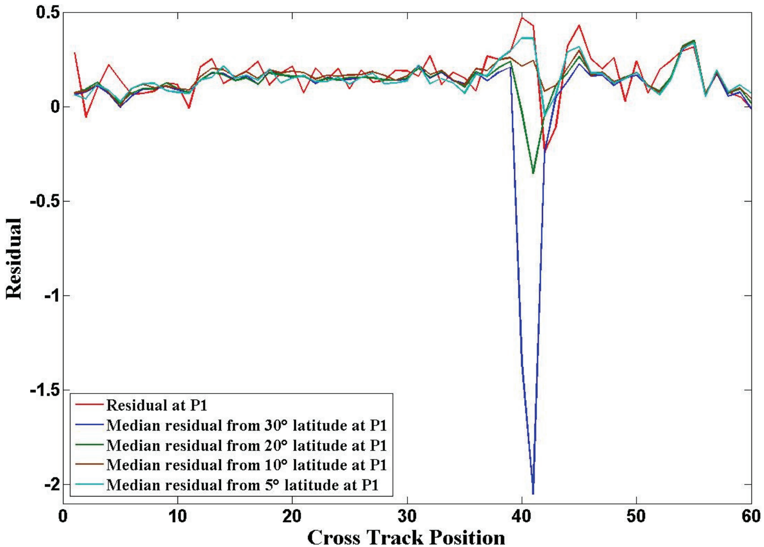

Fig. 5. Residual analysis at the first wavelength pair (orbit 23 909, swath line 1120).

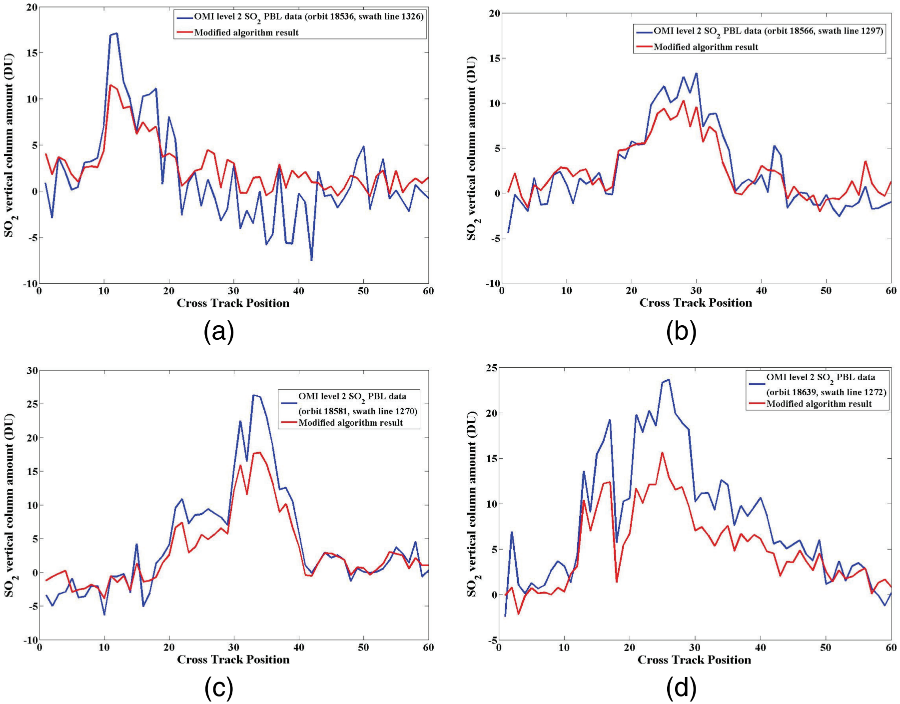

Fig. 6. SO_2 results comparing the OMI level 2 SO_2 PBL data and the modified algorithm result in the cross-track direction: **(a)** 9 January 2008 (orbit 18 536, swath line 1326); **(b)** 11 January 2008 (orbit 18 566, swath line 1297); **(c)** 12 January 2008 (orbit 18 581, swath line 1270); **(d)** 16 January 2008 (orbit 18 639, swath line 1272).

AMTD

5, 979–1001, 2012

AMTD
5, 979–1001, 2012

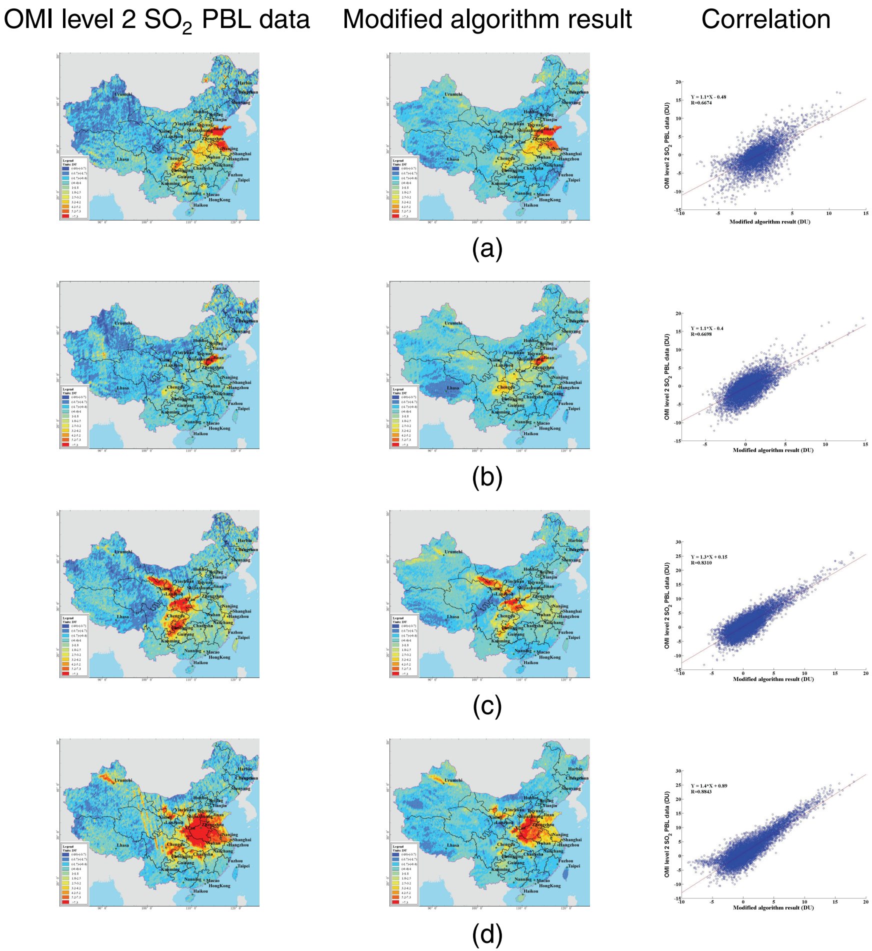

Fig. 7. SO_2 spatial distribution consistency between the OMI level 2 SO_2 PBL data and the modified algorithm result in China: **(a)** 9 January 2008; **(b)** 11 January 2008; **(c)** 12 January 2008; **(d)** 16 January 2008.

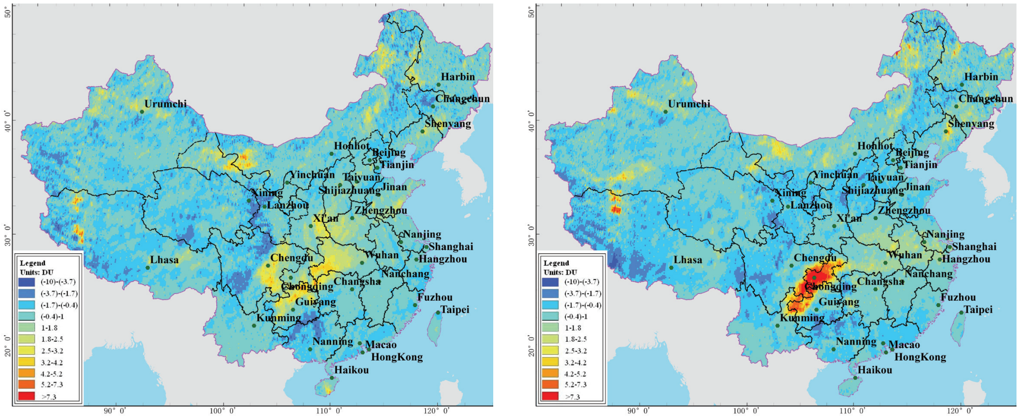

(a) (b)

Fig. 8. Modified algorithm SO_2 result in China: **(a)** 3 January 2009; **(b)** 12 January 2009.